Recognition of the Temperature Condition of a Rotary Kiln Using Dynamic Features of a Series of Blurry Flame Images

Hua Chen, Xiaogang Zhang, Pengyu Hong, Hongping Hu, and Xiang Yin

***Abstract*—Maintaining a normal burning temperature is essential to ensuring the quality of nonferrous metals and cement clinker in a rotary kiln. Recognition of the temperature condition is an important component of a temperature control system. Because of the interference of smoke and dust in the kiln, the temperature of the burning zone is difficult to be measured accurately using traditional methods. Focusing on blurry images from which only the flame region can be segmented, an image recognition system for the detection of the temperature condition in a rotary kiln is presented. First, the flame region is segmented employing a region-growing method with a dynamic seed point. Seven features, comprising three luminous features and four dynamic features, are then extracted from the flame region. Dynamic features constructed from luminous feature sequences are proposed to overcome the problem of mis-recognition when the temperature of the flame region changes rapidly. Finally, classifiers are trained to recognize the temperature state of the burning zone using its features. Experimental results using real datasets demonstrate that the proposed image-based systems for recognizing the temperature condition are effective and robust.**

***Index Terms*—Blurry flame image series, dynamic features, luminous features, temperature condition recognition.**

I. Introduction

THE ROTARY kiln is widely used in metallurgical, refractory material, and chemical industries, such as the cement and aluminum sintering factories. The kiln typically consists of a refractory steel cylinder having a diameter of 4–5 m and a length of about 90–110 m. An aluminum rotary kiln can produce about 500–800 tons of sinter per day. The kiln is rotated continuously by a powerful electrical motor and the temperature in the hottest internal part of the kiln can reach 1400 °C. After a series of physical changes and chemical reactions, the raw materials burned with coal powder inside the kiln are turned into sinter. To achieve the optimum sintering quality, the temperature inside the kiln and especially that in the burning zone has to be controlled within a certain range. The temperature should be high enough to guarantee normal material sintering process. However, if the temperature is too high, materials will be burned sooner than the planned time, and the clinker will become sticky. This condition is referred to as the super-heated condition [1]. In contrast, if the temperature is too low, the materials will not be melt in time and remain solid. This condition is referred to as the super-chilled condition. Super-heated and super-chilled conditions are abnormal conditions that produce inferior products and can even halt production. It is therefore vital to maintain an optimum temperature condition and to avoid temperature fluctuations in a rotary kiln.

The temperature of a kiln is affected by many factors, such as the material load, water content, components of the raw material slurry, and coal heat value. As the temperature varies, the kilnman needs to adjust the quantity of coal fed to control the temperature. Hence, it is essential to accurately measure the temperature in the burning zone. The burning zone in an inclined rotation cylinder is about 10–15 m from the peephole of the discharge port (shown in Fig. 1). The kiln is full of smoke and dust. Conventional temperature measurement systems, such as infrared radiation systems, thermocouple systems, and colorimeter systems, do not work well under such conditions because they are affected by dust and smoke inside the kiln. In addition, it can be difficult to deploy them due to the rotational structure of the kiln. Over the past several decades, the temperature conditions of the rotary kiln are usually judged by the kilnman using the video captured from a digital camera in a manual manner. In recent years, a number of techniques for automatically monitoring and controlling the rotary kiln have been developed to detect abnormal conditions by analyzing thermotechnical signals captured by sensors. Five thermotechnical parameters (including the material feed rate, fuel feed rate, and kiln speed) have been used to build a model for detecting super-heated and super-chilled conditions [1]. A locally linear neuro-fuzzy model has been trained and three distinct models have been developed to detect ringing and coating conditions [2].

Because of the long lag of the complex physicochemical reaction processing in the cylinder, there is a time delay for the thermotechnical-signal-based recognition system. In

Manuscript received September 02, 2014; revised June 30, 2015 and September 20, 2015; accepted October 28, 2015. Date of publication November 17, 2015; date of current version February 02, 2016. This work was supported in part by the Natural Science Foundation of China under Grant 61203016 and Grant 61174050. Paper no. TII-15-0101.

H. Chen and H. Hu are with the College of Computer Science and Electronic Engineering, Hunan University, Changsha 410082, China (e-mail: anneychen@126.com).

X. Zhang and X. Yin are with the College of Electrical and Information Engineering, Hunan University, Changsha 410082, China (e-mail: zhangxg@hnu.edu.cn).

P. Hong is with the Department of Computer Science, Brandeis University, Waltham, MA 02453 USA (e-mail: hongpeng@brandeis.edu).

Color versions of one or more of the figures in this paper are available online at http://ieeexplore.ieee.org.

Digital Object Identifier 10.1109/TII.2015.2500891

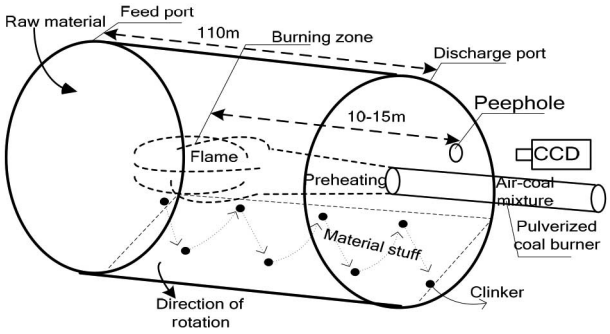

Fig. 1. Motion of granules in the kiln and the sintering process in a rotary kiln.

Fig. 2. CCD installation environment.

recent years, researchers have been exploring image processing techniques for more timely determination of the temperature condition and the feeding control of coal. Image-based methods are quicker and more direct than the thermotechnical-signal-based methods in determining the temperature condition. A set of heterogeneous features and fusion techniques was used to construct a flame-based sinter burning state recognition system [3], which compared ensemble learner models with four types of base classifiers and five fusion operators. First- to fourth-order-statistic hue, saturation and intensity data of the flame image of the rotary kiln were used in a multivariate regression model to measure nitrogen oxides in a rotary kiln [4]. The texture features of the clinker region were used to classify the sintered clinkers into different qualities [5]. Additionally, a five-dimensional feature vector extracted from the material region was used as the input of a robust extreme learning machine (ELM) to recognize the sintering state of a clinker [6]. Temperature distributions and the repose and filling angles were obtained by employing an image processing system and a custom-built infrared camera to optimize the Waelz process for zinc recycling [7].

Most of the image-based methods mentioned above use clear images. The material region can be easily segmented out from the clear image for predicting the temperature conditions using the color and gray-level statistic features of the material region. However, most rotary kilns for cement and aluminum production use coal powder as fuel. They are often full of smokes and dusts because of coal combustion. In our on-site application, most images captured by an industry-grade camera mounted on the discharge port of the kiln are blurry owing to the presence of dust particles in the kiln. The material region in the image is indistinguishable and difficult to be segment out. The most prominent region in a blurry image is the flame region. The flame is formed by the combustion of mixed coal powders and air, so the geometry and intensity of the flame provide instantaneous information of the quality and performance of the burning process. Many techniques that adopt advanced optical sensing, digital image processing, and soft computing algorithms have been developed to study the geometry and intensity of a flame in both laboratory and industrial environments for a variety of applications, especially in the application field of the boiler [8]–[11]. Different from the boiler applications where the temperature of the flame can be detected quantitatively, the nature of a rotary kiln makes quantitative measurement of temperature challenging because of the problem with installing a camera onto the rotational structure of the kiln. Disturbances in image signals due to smokes and dusts also cause severe problems that greatly affect the accurate measurement of the temperature in a rotary kiln.

In this work, we propose a new method for recognizing the temperature condition based on the blurry images obtained from the inside of rotary kilns, from which the material regions cannot be successfully segmented. Seven features (three luminous features and four dynamic features) are extracted from the flame image series, and are used to build a robust and effective condition recognition system for rotary kilns. Section II describes the image acquisition system and segmentation of image. The image features used by the classifier are discussed in Section III. Experimental results are presented in Section IV, which is followed by conclusion in Section V.

II. System Setup and Image Processing

The flowing motion of the granules and the sintering process in the kiln are shown in Fig. 1. During sintering production, raw materials are fed into the kiln from the feed port of the cylinder and coal powder is fed from the discharge port. Generally, a kiln is no more than 30% filled with material. The kiln inclines along its length at an angle to the horizontal of a few degrees and rotates around its axis slowly at a rotation speed of about 1 revolution/60–80 s [12]. The sintering in the kiln is finished with the revolution of the cylinder, and the sinter flows continuously from the feed port to the discharge port as a result of the inclination and rotation of the cylinder. A color charge-coupled device (CCD) camera is installed in the peephole of the discharge port of the kiln (see Fig. 2) and it is in an environment full of suspended coal and dust particles. The output signal of the CCD is digitized using an image grabber card. Each digital image has dimensions of 704×576 pixels, with each pixel having red (R), green (G), and blue (B) components. The sampling frequency of the CCD video camera is 25 frames/s.

Some typical flame image series recorded for a rotary kiln in a large aluminum plant in China are shown in Fig. 3. To segment the flame region out quickly, red, green, and blue (RGB) images are converted to gray-level images first. In practical application, the RGB image is converted to a gray-level image according to [11] by the following equation:

$$I = 0.30R + 0.59G + 0.11B. \quad (1)$$

Fig. 3. Blurred images of the burning zone along the axis of the rotary kiln.

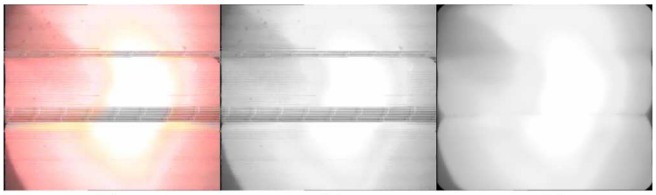

Fig. 4. (a) RGB flame image. (b) Gray-level image I. (c) Denoised image I_g.

There is inherent noise in the flame image acquisition due to dust and interference from the industrial environment. For example, a video signal may be easily disturbed by an electrical fluctuation generated by the ON–OFF operation of the drive motor and by poor contact between the camera and power cable. Fig. 4(a) shows an RGB flame image with stripe interference noise. To reduce noise, a median filter defined as

$$f(x,y) = \text{median}\{I(s,t)\} \quad (s,t) \in S(x,y) \tag{2}$$

is applied to a gray-level image I, where $I(s,t)$ denotes the intensity of a pixel at (s,t) within the mask $S(x,y)$, which is centered on (x,y), and $f(x,y)$ denotes the result after the median filtering. Considering the magnitude of the stripe noise in this paper, the window size of the median filter is 50×50 pixels. Fig. 4(c) shows the denoised image I_g obtained by gray-level image I.

A region-growing method [13] is applied to segment the flame region. As mentioned above, the flame region is located at the center of the image and it is the brightest region in the image. The region-growing algorithm uses a dynamic seed point μ_{seed}, which is determined as follows.

1) The brightest region I_B is found from the pixels whose gray level is greater than B, where B is determined as

$$B = 0.95 \times \max\{f(x,y)\} \quad (x,y) \in I_g. \tag{3}$$

2) The centroid of I_B is then used as μ_{seed}, whose coordinates (x_c, y_c) are computed as

$$x_c = \frac{\sum_{i=1}^{M} f_i(x,y)x_i}{\sum_{i=1}^{M} f_i(x,y)} \tag{4}$$

$$y_c = \frac{\sum_{i=1}^{M} f_i(x,y)y_i}{\sum_{i=1}^{M} f_i(x,y)}. \tag{5}$$

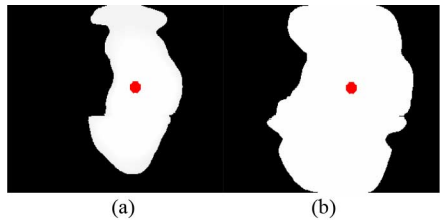

Fig. 5. (a) Brightest region I_B and the seed point. (b) Flame region I_D computed by region growing.

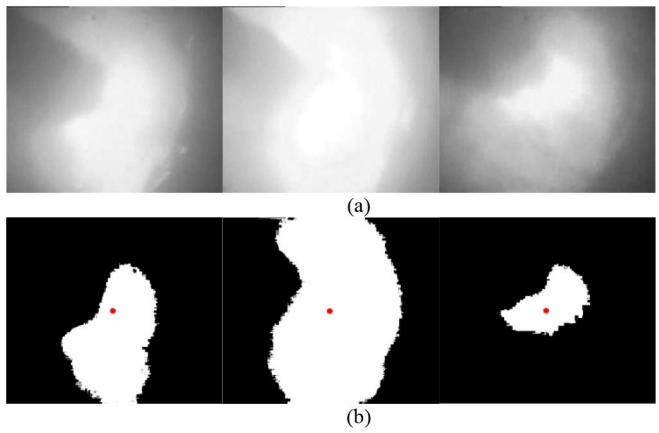

Fig. 6. (a) Gray-level image I_g. (b) Segmented binary images after applying the region-growing algorithm.

The region-growing algorithm gradually incorporates pixels into region I_D if a pixel $f(x,y)$ satisfies the similarity constraint

$$|f(x,y) - \mu_{\text{seed}}| \le T. \tag{6}$$

The threshold $T = 13$ is chosen as the optimal threshold according to experimental results. The segmentation process for the image in Fig. 4(c) is shown in Fig. 5. The segmentation results for the images in Fig. 3 are shown in Fig. 6.

III. Feature Extraction

Feature extraction is vital to the recognition of temperature conditions. According to previous research [14] and the experience of operational experts, two categories of features are extracted from single image and image series to train the classifier for the recognition of the temperature state: luminous features and dynamic features.

A. Luminous Features

Luminous features characterize the luminous intensity parameters of a flame qualitatively and quantitatively to some extent [14]. Luminous features include the average brightness of the flame region, the average brightness of whole image, and flame abundance. They are computed as follows.

1) The average brightness of the flame region is

$$f_1 = G = \frac{1}{H}\sum_{i=1}^{H} f_i(x,y) \quad f_i(x,y) \in I_D \tag{7}$$

where I_D represents the segmented flame region and H is the area of the flame region, which can be computed by counting the number of the pixels falling inside I_D.

2) The average brightness of whole image is

$$f_2 = M = \frac{1}{S}\sum_{i=1}^{S} f_i(x,y) \quad f_i(x,y) \in I_g \tag{8}$$

where I_g is the gray-level image and S is the area of the whole image, which can be computed by counting the number of pixels falling inside I_g. In this paper, the image size is 704×576 pixels, and S is, therefore, 40 504.

3) The flame abundance is

$$f_3 = A = \frac{H}{S}. \tag{9}$$

The flame abundance is the ratio of the area of the flame region to the area of the whole image, and reflects the occupation level of the flame region.

Normally, there is positive correlation between luminous features and the temperature of the kiln. The higher the temperature is, the greater the values of luminous features become. However, there are sometimes exceptions. To explain this problem, a 10-min video of a flame, recorded in the burning zone with a digital video camera at a frame rate of 25 frames per second in an industrial aluminum rotary kiln, was used in the following experiment. The video includes conditions varying from normal to super-chilled, with the super-chilled condition starting at about the 7000th frame. The G, M, and A curves of each frame of the image are shown in Fig. 7. During the first 4 min, the temperature remains normal, and the values of G, M, and, A fluctuate slightly around a mean value, while in the following 6 min, when the temperature decreases, the values fluctuate violently but do not become small. There is no positive correlation between the temperature and the luminous features at this time. It is thus difficult to identify the temperature condition from the luminous features of single image.

There are two main possibilities for the cause of error recognition if only luminous features from a single image are used.

1) When the temperature in the burning zone of a kiln is normal and stable, the coal combustion flame flicks regularly, and the values of the luminous features thus remain relatively stable and fluctuate little. When the temperature varies, especially when it decreases, the flame dances strongly and the values of luminous features fluctuate violently. There is no positive correlation between luminous features and temperature at this time. For example, when the temperature varies, there is sometimes detonation [shown in Fig. 8(a)], which may result in a higher value of the luminous feature extracted from the single flame image at this time, but the real temperature condition is super-chilled.
2) There is much smoke and dust inside the rotary kiln, and inherent noise is readily added to the flame image in the process of acquisition and transmission. This may lead to the inaccurate segmentation of the flame image, and

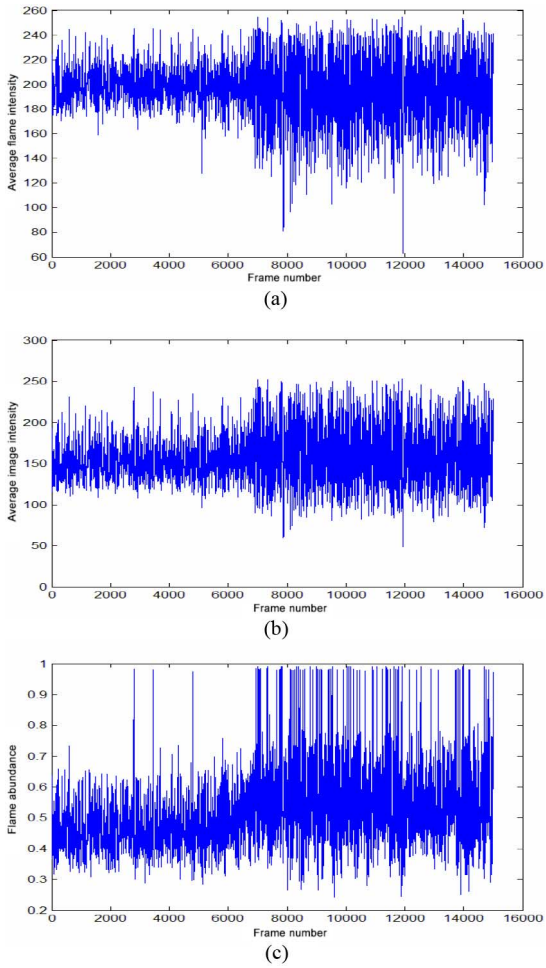

Fig. 7. Luminous feature sequences. (a) $G(i)$ sequence curve. (b) $M(i)$ sequence curve. (c) $A(i)$ sequence curve.

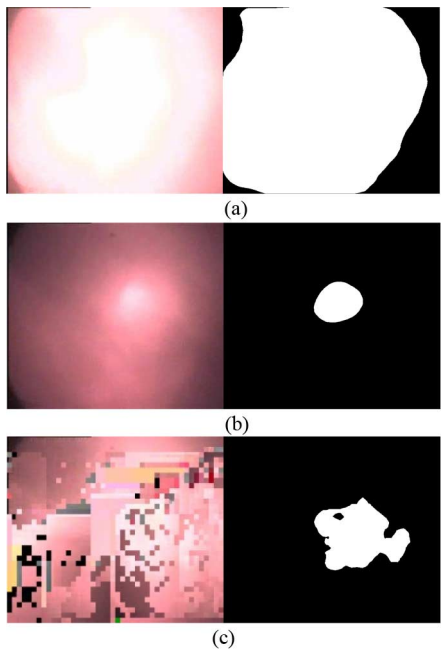

Fig. 8. (a) Detonation image. (b) Image with dust and fog noise. (c) Image with unknown noise.

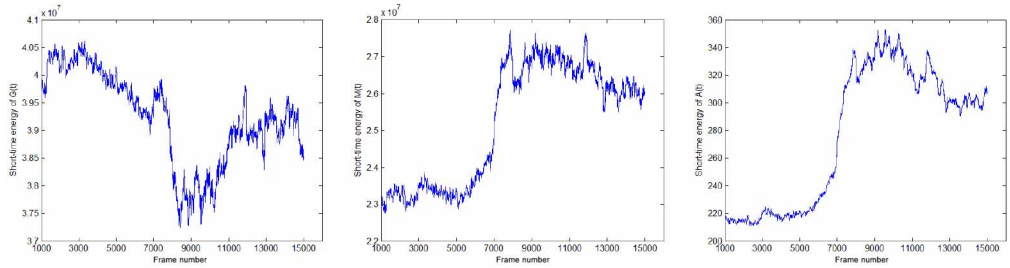

Fig. 9. Short-time energy of (a) $G(i)$, (b) $M(i)$, and (c) $A(i)$.

the luminous features extracted from a single image thus do not reflect the temperature condition exactly. Fig. 8(b) shows an image captured under a normal temperature condition. The flame is obscured by smoke and dust and the flame region cannot be segmented accurately. Fig. 8(c) shows the inaccurate segmentation of images with other unknown noise.

The above discussion demonstrates that luminous features extracted from a single frame of an image are not sufficient for recognition of the temperature condition. Other features are needed to analyze the complex situation. According to the experience of operational experts, the flickering frequency of the flame might be an indication of combustion stability. Therefore, dynamic features could be extracted from the luminous feature sequence of the flame image.

B. Dynamic Features

Dynamic features extracted from the feature sequence include the short-time energy and sample entropy of the luminous feature sequence.

1) Short-Time Energy: Short-time energy is used to distinguish the voiced or silent signal [15], [16] over a long period of time. It is defined as the sum of the squared amplitude of voice samples in a frame. For a data series $\{x(i)\} = x(1), x(2), \ldots, x(n)$, the short-time energy measured at moment t is defined as

$$E_x(t) = \sum_{i=t-(N-1)}^{t} [x(i)w(t-i)]^2 \tag{10}$$

where N is the window width and $w(t-i)$ is the window function. When a rectangular window is used, (10) is simplified as

$$E_x(t) = \sum_{i=t-(N-1)}^{t} x(i)^2. \tag{11}$$

The short-time energy of G ($E_G(t)$) in the tth frame image is computed as follows. (1) The G values of N images $(I(t-N+1), I(t-N+2), \ldots, I(t))$ are computed to form a data sequence $\{G(i)\} = G(t-N+1), G(t-N+2), \ldots, G(t)$. (2) The $E_G(t)$ is computed as

$$E_G(t) = \sum_{i=t-(N-1)}^{t} G(i)^2. \tag{12}$$

$M(i)$ and $A(i)$ sequences are formed in the same manner as the $G(i)$ sequence: $\{M(i)\} = M(t-N+1), M(t-N+2), \ldots, M(t)$ and $\{A(i)\} = A(t-N+1), A(t-N+2), \ldots, A(t)$. The short-time energies of M and A are thus computed as

$$E_M(t) = \sum_{i=t-(N-1)}^{t} M(i)^2 \tag{13}$$

$$E_A(t) = \sum_{i=t-(N-1)}^{t} A(i)^2. \tag{14}$$

In this test, $N = 1000$ is used, and the curves of short-time energy are, therefore, from the 1001th frame to the 15 000th frame. The curves of $E_G(t)$, $E_M(t)$, and $E_A(t)$ are shown in Fig. 9.

For the curve of $E_M(t)$, there is an obvious difference between the first part (1001st–7000th frame) and the latter part (7001st–15 000th frame). The first part is under the normal temperature condition that is associated with higher regularity of $M(i)$, and $E_M(t)$ of the first part is thus smaller than that of the latter part under the super-chilled condition. The trend of $E_A(t)$ is the same as that of $E_M(t)$. So, we take $E_M(t)$ and $E_A(t)$ as f_4 and f_5 of the tth frame.

2) Sample Entropy: Sample entropy (SampEn) is a family of statistics proposed by Richman and Moorman (2000) [17]. It is similar to approximate entropy [18], but it has better precision and is sensitive to changes in the complexity of the data. SampEn quantifies the complexity of time-series data and can be applied to short-length time-series data. It is resistant to short-strong transient interferences (outliers) such as spikes. These characteristics mean that sample entropy is widely used in the nonlinear analysis of time-series data.

For N data from a data series $\{x(i)\} = x(1), x(2), \ldots, x(N)$, two parameters are first defined: m is the embedded dimension of the vector to be formed and r is a threshold, which serves as a noise filter. The sample entropy can be calculated as follows.

1) In sequential order by serial number, a set of m-dimensional vectors is composed as

$$X_m(i) = [x(i), x(i+1), \ldots x(i+m-1)] \quad 1 \le i \le N-m+1. \tag{15}$$

2) $d[X_m(i), X_m(j)]$ is defined as the maximum distance between vectors $x_m(i)$ and $x_m(j)$ and is expressed as

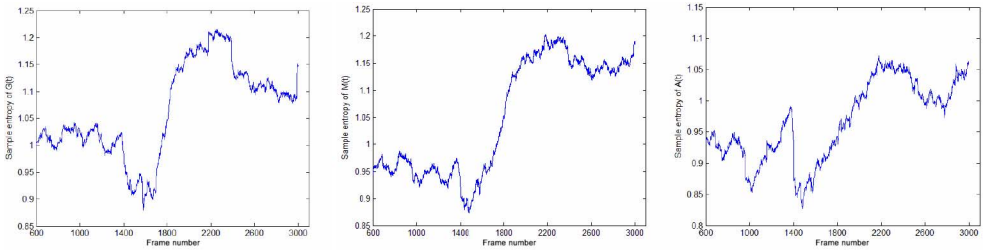

Fig. 10. Sample entropy of $G(i)$, $M(i)$, and $A(i)$.

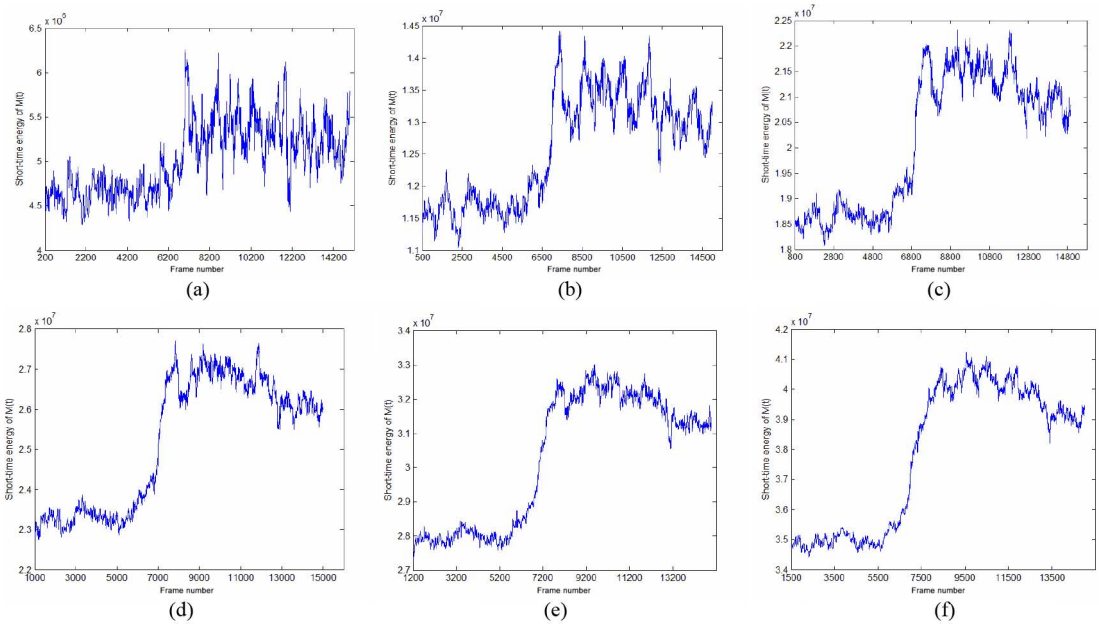

Fig. 11. Curves of $E_M(t)$ with different window widths. (a) $N = 200$. (b) $N = 500$. (c) $N = 800$. (d) $N = 1000$. (e) $N = 1200$. (f) $N = 1500$.

$$d[X_m(i), X_m(j)] = \max_{k=0,\ldots,m-1}(|x(i+k) - x(j+k)|). \tag{16}$$

3) Given a threshold r, for a given $x_m(i)$, the number of j $(1 \le j \le N-m,\ j \ne i)$ is counted, such that $d[x_m(i)x_m(j)] \le r$. This number is denoted B_i and expressed as

$$B_i{}^m(r) = \frac{1}{N-m-1} B_i. \tag{17}$$

4) For parameter m,

$$B^m(r) = \frac{1}{N-m} \sum_{i=1}^{N-m} B_i{}^m(r). \tag{18}$$

5) The number of dimensions is increased as $m = m+1$ and A_i is used to denote the number of $x_{m+1}(i)$ within r of $x_{m+1}(j)$, where j ranges from 1 to $N-m(j \ne i)$. $A_i{}^m(r)$ and $A^m(r)$ are then defined as

$$A_i{}^m(r) = \frac{1}{N-m-1} A_i \tag{19}$$

$$A^m(r) = \frac{1}{N-m} \sum_{i=1}^{N-m} A_i{}^m(r). \tag{20}$$

$B^m(r)$ thus represents the probability that two sequences match for m points, whereas $A^m(r)$ represents the probability that two sequences match for $m+1$ points.

Theoretically, the sample entropy of this sequence $x(n)$ is

$$\text{SampEn}(x) = \ln\left[\frac{B^m(r)}{A^m(r)}\right]. \tag{21}$$

The sample entropy of G ($\text{SampEn}(G(t))$) in the tth frame is computed as follows. 1) The G values of N images $(I(t-N+1), I(t-N+2), \ldots, I(t))$ are computed to form a data sequence $\{G(i)\} = G(t-N+1), G(t-N+2), \ldots, G(t)$. 2) $\text{SampEn}(G(t))$ is computed using (15)–(21). Therefore, the sample entropies of M ($\text{SampEn}(M(t))$) and A ($\text{SampEn}(A(t))$) are computed as $\text{SampEn}(G(t))$ by following steps 1) and 2). The corresponding curves are shown in Fig. 10. The sample entropies of $G(i)$ and $M(i)$ reflect the fluctuation of the feature sequence better. The sample entropies of G_t and M_t are, therefore, used as the features f_6 and f_7.

3) Parameter Selection of Dynamic Features:

a) Window width of short-time energy: Different window widths are used to compute $E_M(t)$, and the relevant curves are shown in Fig. 11. Here, N takes different values, i.e., 200, 500, 800, 1000, 1200, and 1300. When N is larger than 800, the difference between the first half and latter half of a curve is more obvious.

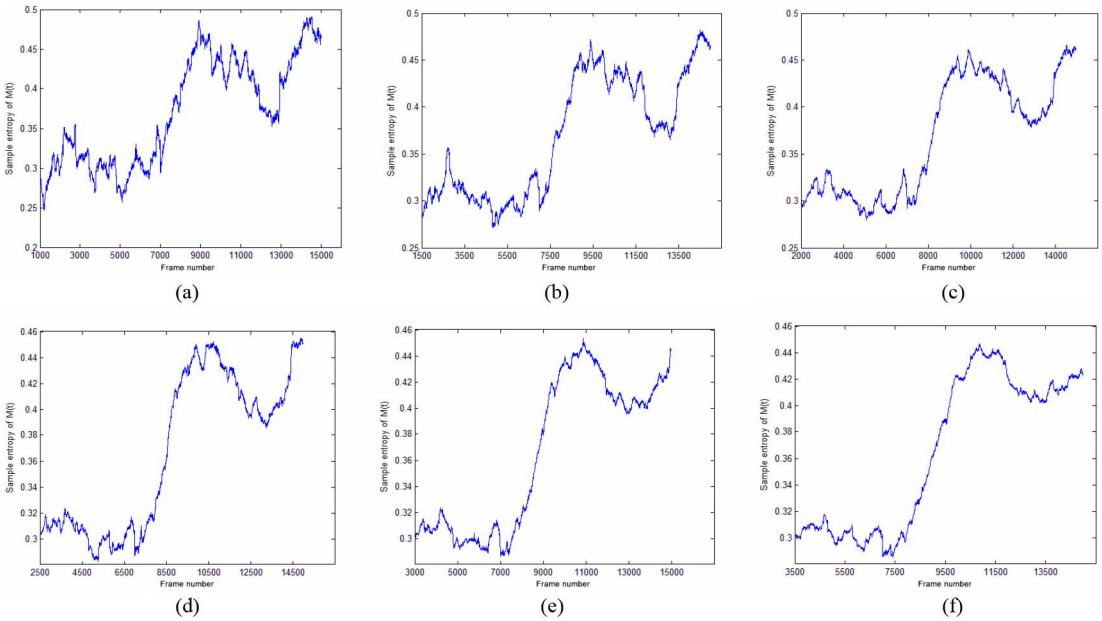

Fig. 12. Curves of SampEn$(M(t))$ with a sampling rate of 25 fps. (a) $N = 1000$. (b) $N = 1500$. (c) $N = 2000$. (d) $N = 2500$. (e) $N = 3000$. (f) $N = 3500$.

TABLE I
SAMPLE ENTROPY COMPUTING TIME WHEN USING DIFFERENT WINDOW WIDTHS N (WITH 25 FPS)

N	1000	1500	2000	2500	3000	3500
Computing time (s)	0.059	0.117	0.193	0.286	0.394	0.536

b) Sampling rate and window width of sample entropy: The value of sample entropy is relevant to the values of m and r, whose selection standards are $r = (0.10 - 0.5)\text{SD}$, $m = 1$ or 2 [19], [20]. Here, SD denotes the standard deviation of the data sequence $x(i)$. This paper uses the parameters $r = 0.5$ and $m = 2$. The window width N is a key parameter for SampEn in different applications. In our experiment, different window widths are used to compute SampEn, and the relevant curves are shown in Fig. 12. Here, N takes different values, i.e., 1000, 1500, 2000, 2500, 3000, and 3500. When N is larger than 2000, there is an obvious difference between the first half and latter half of a curve. Table I gives the different computing times when using different window widths. It is seen that a wider window results in a longer computing time. The test is run on a personal computer with an Intel Core (i3-4150) central processing unit running at 3.5 GHz with 4 GB of RAM.

To speed up the calculation, different sampling rates of data are used for the test. Three-thousand frames are extracted from Fig. 7(b) at a 5-fps sampling rate, and the data curve of $M(i)$ is shown in Fig. 13. Different values of N' (i.e., 200, 300, 400, 500, 600, and 700) are used to compute $\text{SampEn}(M(i))$ in Fig. 13, and the resulting curves are shown in Fig. 14. The corresponding computing are given in Table II. The trend of curves in Fig. 14 is the same as that of curves in Fig. 12 when the parameter N is five times N', but the computing time in Table II is much shorter than that in Table I. Therefore, considering the effect of the computing time, five frames per second is chosen as the sampling rate and the window width N is chosen as 500 for SampEn computing.

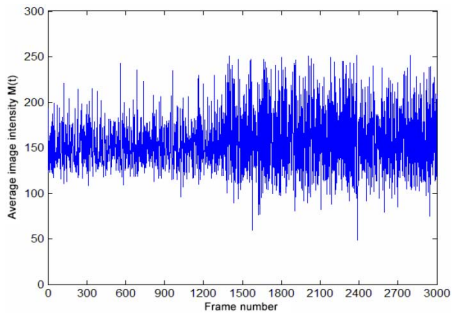

Fig. 13. Curve of $M(t)$ with a sample rate of 5 fps.

The period of temperature condition conversion depends on parameters of the kiln such as components of the raw material slurry, the kiln's bricks and shells, and the coal heat value. Experiments in this paper are based on video collected for no. 6 rotary kiln by the ZhongZhou Aluminum Corporation in China. Therefore, if changing to another rotary kiln, the window width should be adjusted to fit the kiln's parameters.

IV. EXPERIMENTAL RESULTS

Five 10-min videos recorded for the No. 6 rotary kiln of ZhongZhou Aluminum Corporation in China are used as training data. Those videos cover three temperature conditions—normal, super-chilled, and super-heated conditions—as labeled by an experienced kilnman. Image series are extracted from the video at a sampling rate of 5 fps, giving a total of 15 000 typical images extracted from video. Each image has dimensions of 704×576 pixels with an RGB color mode. The features extracted from a single frame and dynamic features obtained from the dynamic features sequence are computed. The parameters of the dynamic feature setting are described in Section III. The window width N is set as 500. Each

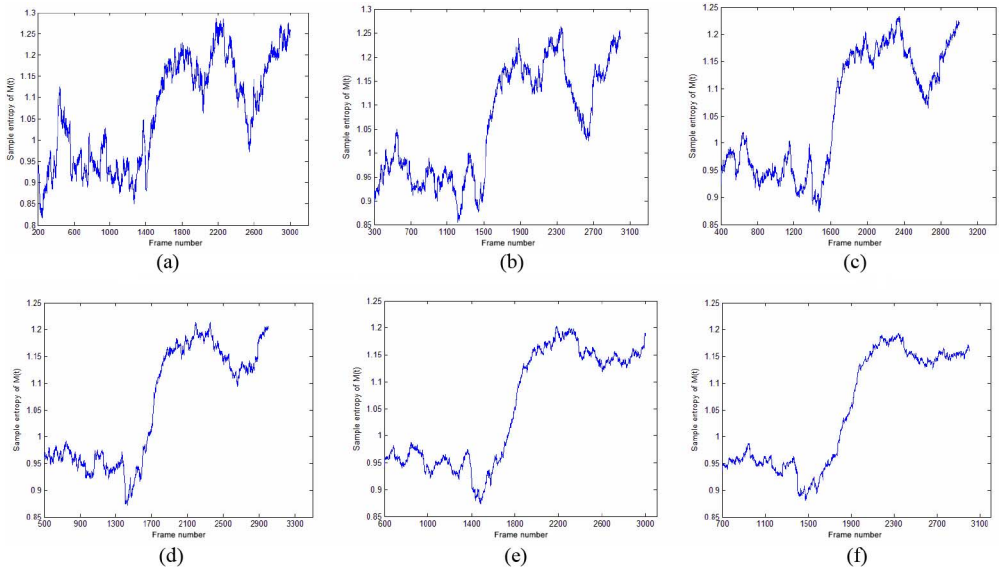

Fig. 14. Curves of SampEn computed from Fig. 13 with a sample rate of 5 fps. (a) $N' = 200$. (b) $N' = 300$. (c) $N' = 400$. (d) $N' = 500$. (e) $N' = 600$. (f) $N' = 700$.

TABLE II
SAMPLE ENTROPY COMPUTING TIME WHEN USING DIFFERENT WINDOW WIDTHS N' (WITH 5 FPS)

N	200	300	400	500	600	700
Computing time (s)	0.008	0.015	0.020	0.030	0.039	0.043

TABLE III
RESULTS OBTAINED USING ELM AND SVM WITH SEVEN FEATURES

	Average accuracy (%)	
	Training	Testing
ELM	87.25	85.43
SVM	87.43	85.65

flame is thus characterized by a vector including seven features $(f_1, f_2, \ldots, f_7)$ and 12 500 training samples are obtained from the image series (2547 samples for super-heated condition, 6386 samples for normal condition, and 3567 samples for super-chilled condition). Test data are taken from another two 10-min videos. Six-thousand frames are extracted from the videos and a total of 5000 testing samples are generated in the same way (1352 samples for the super-heated condition, 2102 samples for the normal condition, and 1546 samples for the super-chilled condition).

Classifiers of an ELM [21] and support vector machine (SVM) [22] are employed to recognize the temperature condition. For the ELM classifier, the activation function used in our paper is sigmoid function $g(x) = 1/(1 + \exp(-x))$. Because the input weights and hidden layer biases of the ELM are chosen randomly, the number of hidden nodes is the only key parameter which is sensitive to the performance. The optimal number of nodes for ELM is selected based on 10-fold cross-validation method. For each tried number of nodes, the training sets are randomly divided into ten subsets of equal size, then one subset is used as validation set which is tested by the classifier trained on the remaining nine subsets. The process is repeated ten times with each of the subset used exactly once as the validation set. The ten results then are averaged to produce a single estimation. The number of hidden nodes is gradually increased from 5 to 100 by interval of 5. Each value is tried based on the above 10-fold cross-validation process and the optimal hidden nodes number of ELM is chosen as 45 for the best cross-validation accuracy. For the SVM, the radial basis function $K(x_i, x_j) = \exp(-\gamma \|x_i - x_j\|^2), \gamma > 0$ is used as kernel function. There are two parameters for SVM needed to be tuned: penalty parameter C and kernel parameter γ. Grid-search using 10-fold cross-validation [23] is implemented to find out the best C and γ. A exponentially growing sequences of $C(2^{-5}, 2^{-4}, \ldots, 2^5)$ and $\gamma(2^{-5}, 2^{-4}, \ldots, 2^5)$ are tried and the optimal parameters are set as $C = 32$ and $\gamma = 16$ for the best cross-validation accuracy. The simulations for ELM are carried out using ELM MATLAB-code package.[1] For SVM compiled C-coded SVM packages, LIBSVM[2] is used. All the simulations for the ELM and SVM algorithms are carried out in MATLAB R2013a environment running on a personal computer with an Intel Core (i3-4150) central processing unit running at 3.5 GHz with 4 GB of RAM.

The final ELM and SVM classifiers are developed using the complete training set. They are retrained with the optimal parameters by all the training datasets and are used to classify the temperature condition on the testing set. Average classification accuracy obtained for 50 trials of two classifiers is given in Table III. Table III shows that both classifiers achieved recognition accuracy of more than 85%. The results demonstrate the effectiveness of the condition recognition system proposed in this paper. The confusion matrix of an SVM classification experiment is shown in Table IV. The classification accuracy of super-chilled (89.3%) is higher than that of normal (85.5%) and super-heated condition (82.9%), because the dynamic feature can represent the fluctuation properties of super-chilled, which cannot be represented by luminous features.

For further comparison, the recognition results achieved with only three luminous features (f_1, f_2, f_3) are given in Table V.

[1] Available: [Online] http://www.ntu.edu.sg/home/egbhuang/elm_codes.html.
[2] Available: [Online] https://www.csie.ntu.edu.tw/~cjlin/libsvm/.

TABLE IV
CLASSIFICATION CONFUSION MATRIX OF SVM

	Super-chilled	Normal	Super-heated
Super-chilled	1381	139	26
Normal	165	1743	194
Super-heated	22	173	1157

TABLE V
RECOGNITION ACCURACY WITH THREE OR FIVE FEATURES (%)

	FEATURES F1-F3		FEATURES F1-F5		FEATURES F1-F3,F6,F7	
	Training	Testing	Training	Testing	Training	Testing
ELM	76.38	75.85	85.81	84.70	84.94	83.29
SVM	76.54	76.23	86.77	85.06	85.65	84.54

The recognition accuracy when using three features is much lower than that when using seven features. The results show the effectiveness of using the seven features chosen in this paper. The experimental results obtained using five features (three luminous features and two dynamic features) are also shown in Table V. Actually, using two dynamic features and luminous features is sufficient for the recognition of a varying condition, especially when using short-time energy. When using the sample entropy with luminous features, because of the time lag of the sample entropy, the testing accuracy is a little lower than that when using short-time energy.

V. CONCLUSION

Determining the temperature in the burning zone is essential to the quality control of sintering of rotary kilns. We have showed that digital blurry images of the burning zones can be used to determine the temperature states of a rotary kiln. It is challenging to segment out the material zone in such blurry images. Our method extracts seven features from the flame region series and uses them to train temperature condition recognizers. Experimental results show that our method is effective and robust. In the future, we will explore the possibility of combining image characteristics with on-site thermo-technical data to better recognize temperature conditions in the burning zone of a rotary kiln.

REFERENCES

[1] I. Makaremi, A. Fatehi, B. N. Araabi, and M. Azizi, "Abnormal condition detection in a cement rotary kiln with system identification methods," *J. Process Control.*, vol. 19, no. 9, pp. 1538–1545, Jun. 2009.

[2] M. Sadeghian and A. Fatehi, "Identification, prediction and detection of the process fault in a cement rotary kiln by locally linear neuro-fuzzy technique," *J. Process Control.*, vol. 21, no. 2, pp. 302–308, Feb. 2011.

[3] W. T. Li, D. Wang, and T. Y. Chai, "Flame image-based burning state recognition for sintering process of rotary kiln using heterogeneous features and fuzzy integral," *IEEE Trans. Ind. Informat.*, vol. 8, no. 4, pp. 780–790, Nov. 2012.

[4] B. Lin and S. B. Jgensen, "Soft sensor design by multivariate fusion of image features and process measurements," *J. Process Control.*, vol. 21, no. 4, pp. 547–553, Apr. 2011.

[5] M. He, J. Zhang, and M. Yan, "Texture analysis and classification for clinker in rotary kiln," in *Proc. Int. Conf. Opt. Photon. Energy Eng.*, May 2010, pp. 211–214.

[6] H. Chen, J. Zhang, X. G. Zhang, and H. P. Hu, "Recognition of sintering state in rotary kiln using a robust extreme learning machine," in *Proc. Int. Joint Conf. Neu. Netw.*, Beijing, China, Jul. 2014, pp. 2563–2570.

[7] J. Matthes, P. Waibel, and H. B. Keller, "A new infrared camera-based technology for the optimization of the Waelz process for zinc recycling," *Miner. Eng.*, vol. 24, no. 8, pp. 944–949, Jul. 2011.

[8] Y. Yan, G. Lu, and M. Colechin, "Monitoring and characterization of pulverized coal flames using digital imaging techniques," *Fuel*, vol. 81, pp. 647–656, Oct. 2002.

[9] G. Lu, Y. Yan, and M. Colechin, "Monitoring of oscillatory characteristics of pulverized coal flames through image processing and spectral analysis," *IEEE Trans. Instrum. Meas.*, vol. 55, no. 1, pp. 226–231, Feb. 2006.

[10] G. Lu and Y. Yan, "Temperature profiling of pulverized coal flames using multicolor pyrometric and digital imaging techniques," *IEEE Trans. Instrum. Meas.*, vol. 55, no. 4, pp. 1303–1308, Aug. 2006.

[11] H. Bae, S. Kim, B. Wang, M. H. Lee, and F. Harashima, "Flame detection for the steam boiler using neural networks and image information in the Ulsan steam power generation plant," *IEEE Trans. Ind. Electron.*, vol. 53, no. 1, pp. 338–348, Feb. 2006.

[12] R. J. Spurling, J. F. Davidson, and D. M. Scott, "The transient response of granular flows in an inclined rotation cylinder," *Chem. Eng. Res. Des.*, vol. 79, no. 1, pp. 51–61, Jan. 2001.

[13] R. C. Gonzalez and R. E. Woods, *Digital Image Processing*, 3rd Ed. Englewood Cliffs, NJ, USA: Prentice-Hall, 2002.

[14] H. L. Yu and J. F. MacGregor, "Monitoring flames in an industrial boiler using multivariate image analysis," *AIChE J.*, vol. 50, no. 7, pp. 1474–1483, Jul. 2004.

[15] L. Lamel, L. Rabiner, A. E. Rosenberg, and J. G. Wilpon, "An improved endpoint dectector for isolated word recognition," *IEEE Trans. Acoust. Speech Signal Process.*, vol. 29, no. 4, pp. 777–785, Aug. 1981.

[16] N. Erdol, C. Castelluccia, and A. Zilouchian, "Recovery of missing speech packets using the short-time energy and zero-crossing measurements," *IEEE Trans. Speech Audio Process.*, vol. 1, no. 3, pp. 295–303, Jul. 1993.

[17] J. Richman and J. Moorman, "Physiological time series analysis using approximate entropy and sample entropy," *Am. J. Physiol. Heart Circ Phys*, vol. 278, no. 6, pp. 2039–2049, Jun. 2000.

[18] S. M. Pincus, "Approximate entropy as a measure of system complexity," *Proc. Natl. Acad. Sci.*, vol. 88, no. 6, pp. 2297–2301, Mar. 1991.

[19] R. Cervigon, C. Sanchez, J. M. Blas, and R. Alcaraz, "Sample entropy analysis of electrocardiograms to characterize recurrent atrial fibrillation," in *Proc. 11th Mediterr. Conf. Med. Biol. Eng. Comput.*, Denmark, Jun. 2007, pp. 54–57.

[20] E. N. Kamavuako, D. Farina, and W. Jensen, "Use of sample entropy extracted from intramuscular EMG signals for the estimation of force," in *Proc. 15th Nordic-Baltic Conf. Biomed. Eng. Med. Phys.*, Denmark, Jun. 2011, pp. 125–128.

[21] G. B. Huang, D. H. Wang, and Y. Lan, "Extreme learning machines: A survey," *Int. J. Mach. Learn. Cybern.*, vol. 2, pp. 107–122, 2011.

[22] V. N. Vapnik, *The Statistical Learning Theory*. Hoboken, NJ, USA: Wiley, 1998.

[23] C. Hsu, C. Chang, and C. Lin. (2003). *A Practical Guide to Support Vector Classification* [Online]. Available: http://www.csie.ntu.edu.tw/~cjlin/

Hua Chen received the B.S., M.S., and Ph.D. degrees in control science and engineering from Hunan University, Changsha, China, in 1996, 2002, and 2014, respectively.

Since 2003, she has been an Assistant Professor with the College of Computer Science and Electronic Engineering, Hunan University. Her research interests include image processing and pattern recognition, machine learning, and computer vision.

Xiaogang Zhang received the Bachelor's, Master's, and Ph.D. degrees in control theory and engineering from Hunan University, Changsha, China, in 1996, 1999, and 2003, respectively.

He is currently a Professor with the College of Electrical and Information Engineering, and the Head of the Department of Automation, Hunan University. His research interests include image process, pattern recognition, and data mining for industrial process applications.

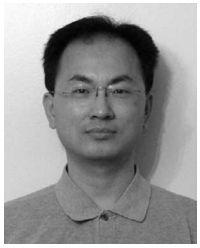

Pengyu Hong received the Bachelor's and Master's degrees in computer science from Tsinghua University, Beijing, China, in 1995 and 1997, respectively, and the Ph.D. degree in computer science from the University of Illinois at Urbana-Champaign, Champaign, IL, USA, in 2001.

After his postdoctoral training in the Department of Statistics and HRP, Stanford University (2002–2004), and the Department of Statistics, Harvard University (2004–2005), he joined Brandeis University, Waltham, MA, USA, as an Assistant Professor of Computer Science in 2005, and was promoted to Associate Professor with Tenure in 2011.

Hongping Hu received the B.S. and M.S. degrees in indusrial automation from Hunan University, Changsha, China, in 1995 and 1998, respectively.

Since 1998, she has been an Assistant Professor with the College of Computer Science and Electronic Engineering, Hunan University. Her research interests include image processing, pattern recognition, and computer vision.

Xiang Yin received the B.S. and M.S. degrees in control science and engineering from Hunan University, Changsha, China, in 1996 and 2006, respectively.

Since 2009, she has been a Senior Engineer with the College of Electrical and Information Engineering, Hunan University. Her research interests include image processing, pattern recognition, and microcomputer system.